Progress In Electromagnetics Research, Vol. 112, 309–327, 2011

SYSTEM ERROR ANALYSIS AND CALIBRATION METHODS FOR MULTI-CHANNEL SAR

L. Ma †

School of Information Engineering
Chang'an University, Xi'an, Shaanxi 710064, China

Z. F. Li and G. S. Liao

National Lab of Radar Signal Processing
Xidian University, Xi'an, Shaanxi 710071, China

Abstract—For multi-channel SAR system, since the minimum antenna area constraint is eliminated, wide swath and high resolution SAR image can be achieved. However, compared to mono-channel SAR system, there exist many deleterious factors in multi-channel SAR system which significantly degrade the quality of SAR image. In this paper, all the deleterious factors in the system are analyzed and classified according to their impact on the SAR imaging processing, in addition an new array error estimation method is presented. The validity of the proposed method is verified by experimental results of measured Tri-channel SAR data.

1. INTRODUCTION

Synthetic aperture radar (SAR) system has been widely used in mapping geological structures and features of stationary scene. With the requirement of surveillance system in civilian and military areas, it is desirable to achieve SAR images with wide swath as well as high resolution A basic limitation for the design of SAR, especially for spaceborne SAR systems is the minimum antenna area constraint which is due to the fact that the illuminated area of the ground must be restricted to assure that the radar does not receive ambiguous returns

Received 8 December 2010, Accepted 12 January 2011, Scheduled 21 January 2011
Corresponding author: Lun Ma (lunma@126.com).
† Also with National Lab of Radar Signal Processing, Xidian University, Xi'an, Shaanxi 710071, China.

in range or/and Doppler. In other words, in order to obtain a high azimuth resolution a wide Doppler bandwidth is required, which is achieved by a long synthetic aperture illuminated by a short antenna in azimuth. Consequently, a high PRF is needed to sample the data in azimuth direction according to the Nyquist criterion. In contrast, a low PRF is favorable to map a wide area unambiguously that is illuminated by a small antenna in elevation.

Some methods [1–6] attempt to address the problem above Unfortunately, they merely obtain a trade-off between the azimuth resolution and illuminated area. To overcome the minimum antenna area constraint, multi-channel SAR system [7–12] has been developed which employ multiple receive-apertures to obtain additional information along the flying track In this system, small transmit-aperture is implemented to illuminate wide area with high resolution, and the receiving antenna is split into multiple sub-apertures with independent receiver channels. Since each individual antenna does not meet the minimum antenna area constraint, range and/or Doppler ambiguities will be inevitably induced into the echoes. In temporal or Doppler domain, a coherent combination of the aliased signals received by all sub-apertures enables a single output signal free of ambiguities. In this way, unambiguous high resolution SAR images of wide area can be obtained ultimately.

It is a hot issue nowadays that a lot of previous works were done to resolve the ambiguities induced by small antennas. The maximum-likelihood (ML) filter and the minimum mean-squared error (MMSE) filter have been used to resolve the range-Doppler ambiguities [7]. A reconstruction algorithm based on the sampling theorem has been investigated to recover the unambiguous Doppler spectrum [8]. A radically different approach has been introduced to resolve the Doppler ambiguities by using spread spectrum waveforms [11]. We have presented a STAP-based approach to resolving the Doppler ambiguities [9, 10]. The main idea of the STAP-based approach will be described in next section.

Under ideal circumstance, all the methods mentioned above can well retrieve the information on ground scene free of ambiguities. However, deleterious factors in multi-channel SAR system seriously degrade the performance of these methods. We have proposed a method for inherent element gain-phase error and along track baseline error estimation [9]. In a real multi-aperture SAR system, more deleterious factors should be considered. These factors mainly include time synchronization error, frequency synchronization error, beam pointing error, baseline error, channel response error, yawing which distorts the along track linear formation of the receive-apertures and

so on. Due to the lack of the real measured multi-channel SAR data, the effects of these errors are rarely considered in the previous works.

In this paper, some main deleterious factors in a multi-aperture system are analyzed in detail and classified by their impact on multi-channel SAR data processing. The error is classified as range-bin misalignment error, spatial steering vector error and coherence error. To cancel the ambiguities as much as possible, the above three kinds of error must be compensated. Furthermore, a robust beamforming method is proposed to mitigate the effect of residual steering vector error. To demonstrate the validity of the proposed method, a set of airborne tri-channel SAR data has been recorded recently. The effectiveness of the approaches for error estimation and aliasing resolving is verified by experimental results of measured data.

This paper is organized as follows: In Section 2, we review the basic properties of multi-channel SAR echo and give the signal model. In Section 3, we make a detailed analysis for main deleterious factors in the system and classify these factors according to their impact on the coherent combination processing. In Section 4, the error estimation method is presented. Subsequently, a robust beamforming method is proposed to mitigate the effect of residual error. In Section 5, some experiments with real measured airborne tri-channel SAR data is given to illustrate the effectiveness of the proposed method. We make conclusions in Section 6.

2. SIGNAL MODELING

The coordinate system of a multi-aperture SAR is defined as follows: X-axis is the direction of the platform velocity vector which is parallel to the ground; Z-axis is away from the ground; Y-axis is perpendicular to the plane constructed by X- and Z-axis; and these three axes form a right-hand and rectangular coordinate.

For a multi-channel SAR system, it is the optimal configuration that all receive-apertures are placed along the flying track. Thus, in this paper, it is assumed that the array is a linear array along the track.

In our experiment, the airborne multi-channel SAR system operates in side-looking and stripmap mode. Figure 1 shows the array model of a multi-channel SAR system where the sub-apertures are on a single platform. Only one sub-aperture in the system is used as the illuminator, and others only receive signals.

To simplify the mathematical model, it is necessary to firstly give the definition of equivalent phase center.

Definition: Two separate transmitting and receiving antennas can be equivalent to a transmitting and receiving antenna which is

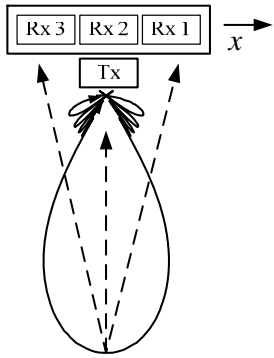

Figure 1. Array model of a multi-channel SAR system.

positioned midway between the separate transmitting and receiving antennas, by compensating a constant phase $\exp\{j2\pi d^2/(4r\lambda)\}$ (where d is the distance between the transmitting and receiving antennas, r is the slant range from the antennas to the ground, and λ is the wavelength of the carrier). In practice, for each range segment only a constant phase needs to be compensated (i.e., r can be approximated to be constant). The position of the equivalent antenna is defined as the equivalent phase center. This definition holds true only when the distance between transmitter and receiver is small enough compared with the distance of the antenna from the ground. It is assumed in this paper that this definition is valid for typical multi-channel SAR system parameters.

It is assumed throughout this paper that the coordinates of each sub-aperture are given according to its equivalent phase center; i.e., every sub-aperture is assumed to both transmits and receives signals, although only one sub-aperture is used as the illuminator.

Assume that the coordinates of the mth ($m = 1, 2, \ldots M$, and M is the number of sub-apertures) sub-aperture are $(x_m, y_m, z_m)((x_1, y_1, z_1) = (0, 0, 0))$ at time $t = 0$. And $(x_m + v_s t, y_m, z_m)$ (where v_s is the platform velocity with respect to the illuminated ground) at time t. The ground echo (two-dimensional) received by the mth sub-aperture at time t can be written as [13, 14]:

$$s_m(t,\tau) = \iint \sigma(x,y,z) h\left(\tau - \frac{2r_m(x,y,z,t)}{c}\right) g\left(t - \frac{x - x_m}{v_s}\right) e^{-j\frac{4\pi r_m(x,y,z,t)}{\lambda}} dxdy + n_m(t,\tau) \quad (1)$$

where

$$r_m(x,y,z,t) = \sqrt{(x - x_m - v_s t)^2 + (y - y_m)^2 + (z - z_m)^2} \quad (2)$$

t and τ denote the azimuth slow-time and range fast-time, respectively; c is the light velocity; $\sigma(x, y, z)$ is the complex reflectivity per unit area (surface scattering) at a ground reflecting cell of which coordinates are (x, y, z), $r_m(x, y, z, t)$ is the slant range from the equivalent phase center of the mth sub-aperture to the ground cell, $h(\tau)$ is the complex transmitted pulse, $g(t)$ represents the antenna pattern and other time-variant characters (identical to all receiving antennas), and $n_m(t, \tau)$ is the additive complex white noise.

Transforming (1) into the Doppler domain (using the stationary phase method), yields:

$$S_m(f_d, \tau) = e^{j2\pi f_d x_m / v_s} A(f_d, \tau) + N_m(f_d, \tau) \tag{3}$$

where

$$A(f_d, \tau) = \iint \sigma(x, y, z) h\left(\tau - \frac{2r(x, y, z, f_d)}{c}\right) G(f_d) e^{-j\psi(x,y,z,f_d)} dxdy \tag{4}$$

$$\psi(x, y, f_d) = \frac{4\pi\sqrt{(y-y_m)^2 + (z-z_m)^2}}{\lambda} - \frac{\pi\lambda\sqrt{(y-y_m)^2 + (z-z_m)^2} f_d^2}{2v_s^2} + 2\pi f_d \frac{x}{v_s} \tag{5}$$

f_d is the instantaneous Doppler frequency, $G(f_d)$ and $N_m(f_d, \tau)$ are the Fourier transformations of $g(t)$ and $n_m(t, \tau)$, respectively.

In our experiment, the tri-channel SAR system operates at X-band, the wavelength $\lambda = 3$ cm. A waveguide slot antenna array [15–17] with 3 sub-apertures is implemented in the system for receiving signals, thus $M = 3$ in our experiment. And each sub-aperture receives the echoes of the transmitted pulse from the ground cells. The received RF waveforms are coherently quadrature demodulated in each receiver. The width of each sub-aperture along the flying track is 0.552 meters, and the distance between each two adjacent sub-apertures is 0.559 meters. The carrier velocity v_s is 120 meters per second. The 3 dB Doppler bandwidth is about 450 Hz. To retrieve the clutter spectrum as wide as possible but not merely 3 dB bandwidth, it is assumed that the Doppler frequencies f_d of the ground cells illuminated by the antenna mainlobe are confined within about $[-300, 300]$ Hz. For a SAR system, the relationship between the Doppler frequency f_d of each ground stationary cell and its corresponding cone angle ϕ can be written as [18, 19].

$$f_d = 2v_s \sin\phi / \lambda \tag{6}$$

Consequently, the clutter spectrum can be shown by the thick line in the $f_d - \sin\phi$ plane of Figure 2(a).

To verify the effectiveness of the approaches for resolving Doppler aliasing, lower pulse repetition frequency (PRF) is adopted

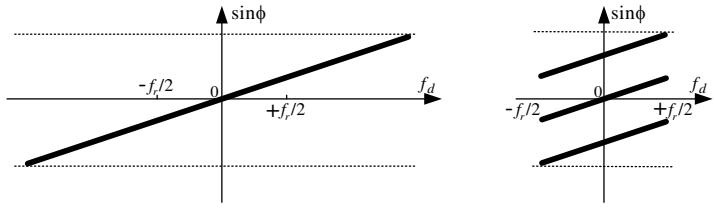

(a) Doppler unambiguous (b) Doppler ambiguous

Figure 2. Space-time spectrum of ground echoes.

intentionally in the experiment. Here PRF $f_r = 200\,\text{Hz}$. The lower PRF will introduce azimuth (Doppler) ambiguities for each small receiving antenna. There exist three azimuth angles for the same Doppler frequency f_d, as shown by the three thick lines in Figure 2(b).

Without loss of generality, the example shown in Figure 2(b) is used in the following mathematical description. Considering the Doppler ambiguities and using (6), we can modify (3) as

$$S_m(f_d,\tau) = \sum_{i=-1}^{1} e^{j4\pi x_m \sin\phi_i(f_d)/\lambda} A_i(f_d,\tau) + N_m(f_d,\tau) \tag{7}$$

where

$$\sin\phi_i(f_d) = \lambda(f_d + if_r)/2v_s \quad (i=-1,0,1) \tag{8}$$

$$A_i(f_d,\tau) = A(f_d + if_r,\tau) \quad (i=-1,0,1) \tag{9}$$

The value range of f_d in (7), (8) and (9) is $[-f_r/2,\, f_r/2]$ (due to the lower PRF sampling). It is clarified by (7), (8) and (9) that there are three are three cone angles (ϕ_{-1}, ϕ_0 and ϕ_1) for the same Doppler frequency f_d.

The output $S_m(f_d,\tau)$ $(m = 1,2,\ldots,M)$ from the range-Doppler bin $\tau - f_d$ can be expressed using vector notation as follows:

$$\mathbf{s}(f_d,\tau) = \mathbf{P}(f_d)\cdot\mathbf{a}(f_d,\tau) + \mathbf{n}(f_d,\tau) \tag{10}$$

where

$$\mathbf{s}(f_d,\tau) = [S_1(f_d,\tau), S_2(f_d,\tau), \ldots S_M(f_d,\tau)]^T \tag{11}$$

$$\mathbf{P}(f_d) = [\mathbf{p}_{-1}(f_d), \mathbf{p}_0(f_d), \mathbf{p}_1(f_d)]^T \tag{12}$$

$$\mathbf{p}_i(f_d) = \left[1, e^{j4\pi x_2 \sin\phi_i(f_d)/\lambda}, \ldots e^{j4\pi x_M \sin\phi_i(f_d)/\lambda}\right]^T \tag{13}$$

$$\mathbf{a}(f_d,\tau) = [A_{-1}(f_d,\tau), A_0(f_d,\tau), A_1(f_d,\tau)]^T \tag{14}$$

$$\mathbf{n}(f_d,\tau) = [N_1(f_d,\tau), N_2(f_d,\tau), \ldots N_M(f_d,\tau)]^T \tag{15}$$

Due to the existence of ambiguities of the Doppler spectrum, as shown in Figure 2(b), the quality of SAR image is degraded seriously. We have presented a STAP-based approach to recover unambiguous Doppler spectrum [9, 10]. The main idea of the proposed method can be concluded as follows: firstly the ground echoes received by each sub-aperture can be divided into many spectrum components in the $f_d - \sin\phi$ plane, each of the spectrum components is confined into a narrower angle range. And the three aliasing spectrum components existing in the same Doppler frequency correspond to three different spatial angles. According to this fact, we can extract the ambiguous spectrum components separately by using spatial beamforming technique. After the operation above is performed for each Doppler frequency, the whole Doppler spectrum can be finally recovered.

3. ERROR ANALYSIS AND CLASSIFICATION

In this section, we firstly focus on the factors which influence the performance of resolving Doppler ambiguities. By analyzing these factors, main error sources in multi-aperture SAR system are classified.

Due to the fact that all aliased components in Doppler domain can be separated in spatial domain, as has been pointed out, we can extract each spectrum component by steering the spatial beam to the direction of it. And the adaptive weight vector is generated by multi-aperture returns and the steer vector of the aliasing component [10]. Consequently, if there are perturbations in the steering vector defined by Eq. (12), the spatial beam can not be steered to the aliasing component accurately. It is certain that with steer vector error Signal Noise Ratio (SNR) loss increases.

As has been described in section, Doppler aliasing is resolved in Range-Doppler domain. In the direction of cross-range, Doppler spectral envelopes of different ground cells for the same range bin are automatically aligned after azimuth FFT performed. Theoretically, all receivers should have the same range bins at the same receiving position along the flying track so that the output $S_m(f_d, \tau)$ $(m = 1, 2, \ldots, M)$ of each channel from the range-Doppler bin $\tau - f_d$ represents the same ground cells. It is the prerequisite for resolving Doppler aliasing. However, for a real multi-channel system, the requirement above is limited by range-bin misalignment. In the condition that each receiver has different range bins, Doppler ambiguities can not be restrained effectively.

In addition, to resolve Doppler ambiguities we combine the multi-channel data coherently, the coherence of the data must be high

enough. Otherwise the performance of data processing will degrade accordingly.

According to the explanations above, the impact on resolving Doppler ambiguities may be classified into these three kinds as follows:

The first kind: the clutter spectrums of all channels are not aligned in the direction of range, i.e., the echo delay times of all channels are different from each other at the same receiving position along the flying track. This kind of error is referred to as ***range-bin misalignment error***.

This kind of error rises from time synchronization error, frequency synchronization error and cross-track baseline error caused by yawing.

Time synchronization error is the inconsistency of system pulse triggering time, which results in different echo delay times.

Frequency synchronization error is the inconsistency between carrier frequency and receiver local oscillator. Fixed frequency error causes the migration of the target profile along the cross track. It should be noted that high order frequency error may extend the target profile and raise the side lobe.

Yawing means that the flying path of the platform is not a straight line, which leads to a cross-track baseline. Clearly, different receiving positions cross the track result in range-bin misalignment error.

The second kind: the spatial steering vector of aliasing component is not accurate, i.e., ***steering vector error***.

This kind of error rises from inherent element gain-phase error, baseline error.

Inherent gain-phase error is caused by channel mismatch. Gain error can be automatically compensated during adaptive processing due to the fact that the array weights are adaptively computed for each range-Doppler bin corresponding to a small portion of beam patterns. However, phase error deteriorates the performance of resolving Doppler ambiguities seriously.

Baseline error is the difference between the receiving position of each channel and its measured value (x_m, y_m, z_m). Define the position error as $(\Delta x_m, \Delta y_m, \Delta z_m)$. And baseline error may be classified as along-track baseline error (i.e., Δx_m) and cross-track baseline error (i.e., Δy_m and Δz_m). It can be noted according to Eq. (12) that steering vector mainly depends on the along-track baseline when other parameters are fixed. In addition, cross-track baseline error can be equivalent to a gain-phase error in the condition that the cross-track baseline is short enough [9]. After the above simplification, now we only need to estimate two errors: the gain-phase error and the position error along the track.

The third kind: reduced coherence results in performance

degradation of resolving Doppler aliasing, which is referred to as ***coherence error****.*

This kind of error rises from beam synchronization error, channel response error.

Beam synchronization error mainly refers to beam pointing error. It indicates that the beam illuminating center of each channel does not point to that of reference channel. Beam pointing error is mainly caused by the attitude error of platform which includes rolling, pitching and yawing error. Rolling error only reduces the common illuminating area in the direction of range. But pitching and yawing error lead to different Doppler centers of receiving channels, which leads to antenna pattern modulation mismatch. Furthermore, it reduces the coherence of multi-channel data.

Channel response error means that the frequency responses of receiving channels in the system are different from each other, which reduces the coherence of multi-channel data as well.

As mentioned above, although there are many error sources in a real multi-channel SAR system, according to the their impact on the performance of resolving Doppler aliasing, these error sources can be concluded as range-bin misalignment error, steering vector error and coherence error. Thus only three kinds of error need to be considered, and there is no need to estimate each of the error source mentioned above. The analysis above simplifies the implementation of error estimation. In the next section, we will introduce the methods of estimating these three kinds of error in detail.

4. ERROR ESTIMATION AND COMPENSATION

In this section, we firstly present the error estimation method. Subsequently, a robust beamforming method is proposed to mitigate the effect of residual error.

4.1. Range-bin Misalignment Error Estimation

As has been described, the Doppler spectrum is divided into many spectrum components in the $f_d - \sin\phi$ plane by azimuth FFT operation, and each aliasing Doppler spectrum component corresponds to different spatial angle. For each range-Doppler bin, the ambiguous spectrum components can be extracted by steering the spatial beams to them respectively.

It is the prerequisite for a coherent combination of the aliased signals received by all sub-apertures that all receivers have the same range bins at the same receiving position along the flying track. In

other words, the spectrum components to be extracted of each channel must correspond to the same clutter patch.

With range-bin misalignment error, the multi-channel data vector $\mathbf{s}(f_d, \tau)$ will change to $[S_1(f_d, \tau_1), S_2(f_d, \tau_2), \ldots S_M(f_d, \tau_M)]^T$. So that aliasing components can not be extracted and rejected completely. Thus, the range bin needs to be corrected before resolving Doppler aliasing.

Here, the envelope correlation function is used to estimate the range-bin shift between the two channels in the system. However, the coherence of the pulses for correlation function generation must be taken into account.

In fact, even the pulses received by two adjacent apertures at the same time, do not illuminate the same ground cells due to their different receiving positions along the flying track. To improve the coherence of the returns between every two channels before range-bin alignment, we need to select pulses with much nearer receiving positions. In practical processing, we may delay the pulses received by each sub-aperture in slow time (azimuth time) domain. By doing this, the receiving apertures can be compressed into a short array along the track with the maximum length of $v_s T_r$. The demonstration of this operation is given in the following.

Without loss of generality, x_m $(m = 1, 2, \ldots, M)$ can be decomposed into the following two parts:

$$x_m = k_m v_s T_r + \delta x_m \tag{16}$$

where k_m is an integer, T_r is the pulse repetition period and $0 \leq \delta x_m \leq v_s T_r$. Accordingly we may appropriately delay the pulses received by each channel in slow time (azimuth time) domain to obtain the compressed array; i.e., the pulses received by the mth aperture are delayed by $k_m T_r$. We refer to the short array with the element positions (along-track) of $[0, \delta x_2, \ldots, \delta x_M]$ as the compressed array in this paper. The time delay of the pulses is equivalent to the change of the along-track position from x_m to $\delta x_m = x_m - k_m v_s T_r$. The operation above is equivalent to selecting the nearest sampling positions of receiving apertures. This, it should be noted, is more important for a large along-track linear array. The nearer the spatial sampling positions, the higher the coherence of the pulses.

In the next step, the pulses received by each aperture are pulse compressed in fast time domain. To improve the estimation precision, we perform interpolation operation to each range profile. After that, range bins are aligned according to the correlation feature of the interpolated echo envelopes [20]. Considering the spatially-variant characteristic of range-bin misalignment, we may divide the pulse returns into several blocks along the track. By averaging the estimates

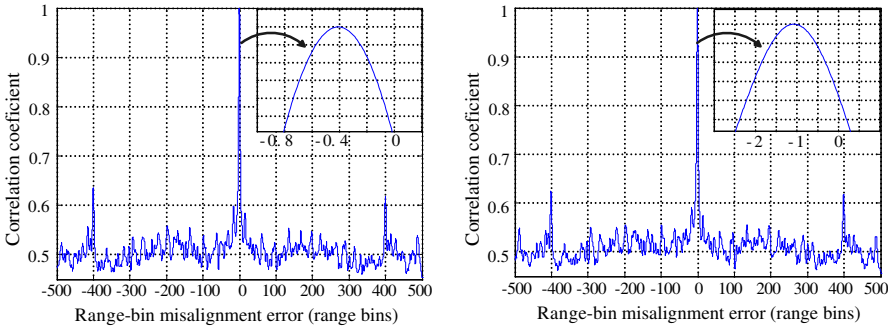

(a) Channel 2 (b) Channel 3

Figure 3. Correlation coefficient.

of range-bin misalignment error, the precision can be further improved. The estimation result of this set of tri-channel measured data is given in following. Figure 3(a) illustrates the correlation coefficient (100 times interpolation) between channel 2 and reference channel (namely channel 1). Figure 3(b) shows the correlation coefficient between channel 3 and channel 1. After average operation, the range-bin misalignment error of the two channels is 0.43 and 1.12 range bins, respectively.

4.2. Steering Vector Calibration

The ambiguous spectrum components can be extracted by steering the spatial beam to one of them and form nulls to the others. The operation above needs the steering vector to be known accurately. The SNR of the extracted spectrum component is closely bound up with the precision of the steering vector. By (12), we can see that the precision of steering vector mainly depends on the estimation accuracy of the baseline. It has been indicated by us that the estimate of baseline error level should be less than one centimeter at X-band [9]. It is quite difficult to satisfy the requirement above only by measuring instruments. And considering the channel mismatch, inherent gain-phase error also leads to the degradation of the precision of the steering vector seriously. Thus, in the presence of the errors above, the steering vector of the aliasing component with error can be rewritten as:

$$\begin{aligned}&\hat{\mathbf{p}}_i(f_d)\\ &= \left[1, g_2 e^{j\zeta_2} e^{j4\pi(x_2+\Delta x_2)\sin\phi_i(f_d)/\lambda}, \ldots g_M e^{j\zeta_M} e^{j4\pi(x_M+\Delta x_M)\sin\phi_i(f_d)/\lambda}\right]^T\\ &= \mathbf{\Gamma}\mathbf{p}_i^{,}(f_d)\end{aligned} \tag{17}$$

where

$$\mathbf{\Gamma} = \mathrm{diag}\left\{1, g_2 e^{j\zeta_2}, \ldots, g_M e^{j\zeta_M}\right\} \tag{18}$$

$$\mathbf{p}_i^{'}(f_d) = \left[1, e^{j4\pi(x_2+\Delta x_2)\sin\phi_i(f_d)/\lambda}, \ldots e^{j4\pi(x_M+\Delta x_M)\sin\phi_i(f_d)/\lambda}\right]^T \tag{19}$$

where $g_m e^{j\zeta_m}$ $(m = 1, 2, \ldots M)$ is the gain-phase error of the mth array element. And Δx_m $(m = 1, 2, \ldots M)$ is the position error of the mth array element along the flying track. diag$\{\cdot\}$ denotes matrix diagonalization operation. In addition, cross-track baseline error can be modeled as a phase error when it is short enough [9].

After the above simplification, now we only need to estimate two errors: the gain-phase error (i.e., $g_m e^{j\zeta_m}$) and the position error along the track. As mentioned in Section 2, the spectra of all ground stationary reflecting cells are superimposed in the space-time plane after performing the azimuth FFT transformation, as formulated by (7). Due to Doppler aliasing, for each range-Doppler bin there are three spectrum components with different spatial angles. Since the angles of the aliasing spectrum components are known exactly, all these three components can be taken as the calibration sources. Consequently, both $\mathbf{\Gamma}$ and Δx_m can be estimated by using self-calibration method. The method of estimating $\mathbf{\Gamma}$ and Δx_m will be given in following.

Firstly the covariance matrix, denoted as $\mathbf{R}(f_d, \tau)$, associated with the array output vector from the range-Doppler bin $\tau - f_d$ is given by $\mathbf{R}(f_d, \tau) = E\{\mathbf{s}(f_d, \tau)\mathbf{s}^H(f_d, \tau)\}$, $E\{\}$ represents the statistical averaging. In practice, the statistical covariance matrix $\mathbf{R}(f_d, \tau)$ can be estimated by the sample covariance matrix, and the samples can be easily obtained from range bins (i.e., range samples). The sample covariance matrix $\hat{\mathbf{R}}(f_d, \tau)$ can be calculated by

$$\hat{\mathbf{R}}(f_d, \tau) = \frac{1}{2K+1} \sum_{k=-K}^{K} \mathbf{s}(f_d, \tau - K/2 + k)\mathbf{s}^H(f_d, \tau - K/2 + k) \tag{20}$$

where $2K+1$ is the number of samples used to estimate the covariance matrix. Reed et al. have shown that $2K + 1 \geq 2M - 1$ is a rule for a 3 dB loss due to estimation [21, 22]. $(\cdot)^H$ denotes the vector conjugate-transpose operation.

Assuming the additive noise at each array element is independent and white, the covariance matrix can be decomposed as [21, 22]

$$\hat{\mathbf{R}}(f_d, \tau) = \sum_{l=1}^{L} \lambda_l \beta_s^{(l)} \beta_s^{(l)H} + \sum_{j=1}^{M-L} \lambda_{j+K} \beta_n^{(j)} \beta_n^{(j)H} \tag{21}$$

where L is the number of ambiguities within each Doppler bin. The eigenvalues satisfy $\lambda_1 \geq \lambda_2 \geq \ldots \lambda_L \gg \lambda_{L+1} \geq \ldots \geq \lambda_M$, eigenvectors $\beta_s^{(l)}$ $(l = 1, \ldots L)$ associated with the larger eigenvalues λ_l $(l = 1, \ldots L)$ span the signal subspace. And eigenvectors $\beta_n^{(j)}$ $(j = 1, \ldots, M - L)$ associated with the smaller eigenvalues λ_j $(j = 1, \ldots, M - L)$ span the noise subspace.

It is known that the real spatial steering vectors $\mathbf{p}_i(f_d)$ also span the signal subspace as $\mathbf{U}_S = [\beta_s^{(1)}, \beta_s^{(2)}, \ldots \beta_s^{(L)}]$ does, thus $\mathbf{p}_i(f_d)$ should be orthogonal to each column of matrix $\mathbf{U}_N = [\beta_n^{(1)}, \beta_n^{(2)}, \ldots \beta_n^{(M-L)}]$. Then, we can define cost function as:

$$J_c = \hat{\mathbf{p}}_i^H(f_d)\mathbf{U}_N\mathbf{U}_N^H\hat{\mathbf{p}}_i(f_d) \tag{22}$$

The estimate of $\mathbf{p}_i(f_d)$ can be obtained by minimizing the cost functionJ_c.

Define the position error vector along the track as $\mathbf{\Delta x} = [\Delta x_1, \Delta x_2, \ldots \Delta x_M]^T$. The estimate algorithm comprises two steps. In the first step, fixing $\mathbf{\Delta x}$ (initial value is zero); we estimate the gain-phase error $\mathbf{\Gamma}$ of each array element. In the second step, using the result of the first step, i.e., holding the gain-phase error fixed, we estimate $\mathbf{\Delta x}$. The algorithm iterates alternatively between the two steps to find the final solution.

It should be noted that there are only three channels in this experiment (i.e., $M = 3$) and the Doppler spectrum is also aliased three times (i.e., $L = 3$). Due to the fact above, the dimension of noise subspace (ML) will be zero. For the sake of verification of the validity of the proposed method, we set the PRF of reference channel as 400 Hz before experiment (while the PRF of the other two channels is 200 Hz). In this way, we can obtain a new channel by downsampling the pulses received by channel 1 (reference channel). The new channel generated by downsampling operation is referred to as channel 4 (i.e., $M = 4$ in this step).

After the above downsampling operation, we can verify the validity of the self-calibration method. Here gain error is measured in dB; phase error is measured in degrees and position error is measured in millimeters, respectively. To estimate the covariance of matrix of (20), two hundred samples were used. All the samples were obtained from two hundred adjacent range bins. The estimate of gain error of channel 2 and channel 3 corresponding to channel 1 (the reference channel) are 3.64 dB and 4.51 dB (i.e., g_2 and g_3), respectively. The estimate of phase error of channel 2 and channel 3 corresponding to channel 1 are 11.2° and -116.15° (i.e., ζ_2 and ζ_3), respectively. And the estimate of position error along the track of channel 2 and channel 3 corresponding

to channel 1 are 2.3 millimeters and 1.6 millimeters (i.e., Δx_2 and Δx_3), respectively. Since channel 4 is generated by downsampling operation the estimate of the gain error, phase error and position error of channel 4 corresponding to reference channel are all zero, respectively.

4.3. Coherence Error

As mentioned in Section 3, although reduced common illuminating area in the direction of range caused by rolling error does not impact the processing result of resolving Doppler aliasing system, the uncommon part of clutter spectrum for different channels caused by beam pointing error will inevitably degrade the coherence of multi-channel SAR data [23]. In a conventional multi-channel SAR system, to improve the coherence of data we may remove the uncommon clutter spectrum of each channel in the directions of range and azimuth, respectively.

For a small aperture multi-channel SAR system, the method mentioned above can not be adopted directly in the direction of azimuth due to Doppler aliasing. Before resolving Doppler aliasing, both the common part and the uncommon part of Doppler spectrum is aliased. Thus it is difficult to extract or remove both of them at this time. In this case, beam pointing error must be compensated before data recording [24]. In addition, channel response error is suggested to be compensated by channel equalization technique [26, 27] due to its time and spatial variation characteristic. The experimental results shown in next section confirm the validity of the adopted methods

4.4. A Robust Method to Mitigate the Effect of Residual Error

In Section 4.2, we have described the method of estimating steering vector error on the basis of orthogonality between noise subspace and real steering vector. However, there may still be residual error due to inaccurate noise subspace estimation which is usually caused by low independent and identically distribution (i.i.d) of samples for estimating covariance matrix or small dimension of noise subspace. In our experiment, the dimension of noise subspace is only 1 due to system limitations. The problem above must be taken into account, because we estimate the error just by employing the characteristic of steering vector orthogonal to the noise subspace, An approach for mitigating the effect of residual error is given in the following.

For better error tolerance, adaptive method is implemented to cancel Doppler ambiguities in our former paper [10]. But the adaptive weight vector for aliasing rejection in a multi-channel SAR data may still be sensitive to residual error. For the convenience of explanation,

we rewrite the adaptive weight vector for resolving Doppler aliasing as:

$$\begin{aligned}\mathbf{w}(f_d,\tau)&=\hat{\mathbf{R}}(f_d,\tau)^{-1}\hat{\mathbf{p}}_i(f_d,\tau)\\&=\left[\hat{\mathbf{p}}_i(f_d,\tau)-\sum_{l=1}^{L}\left(\frac{\lambda_l-\lambda_{\min}}{\lambda_l}\right)\beta_s^{(l)}\beta_s^{(l)H}\hat{\mathbf{p}}_i(f_d,\tau)\right]/\lambda_{\min}\end{aligned}\quad(23)$$

Assume $\lambda_{L+1}\approx\lambda_{L+2}\ldots\approx\lambda_M=\lambda_{\min}$. The description above shows the formation process of adaptive weight vector. Since $\mathbf{U}_S=[\beta_s^{(1)},\beta_s^{(2)},\ldots,\beta_s^{(L)}]$ (in our experiment $L=3$) spans the same subspace (i.e., signal subspace) as the real steering vectors $\mathbf{p}_i(f_d,\tau)$ $(i=-1,0,1)$ does, the second item of (23) can form nulls at the directions of all aliasing components adaptively certainly including the signal to be extracted. In other words, the samples for estimating covariance matrix $\hat{\mathbf{R}}(f_d,\tau)$ which does not contain the component to be extracted can prevent the component being canceled, even in the condition that the steering vector is inaccurate. But we can not obtain such samples whatsoever, because there always exist three azimuth angles for the same Doppler frequency as shown in Figure 2(b). To mitigate SNR loss of the extracted component, all we can do is to obtain more accurate steering vector.

As mentioned above, residual error is usually caused by inaccurate noise subspace estimation. And we estimate steering vector error in section B just by making use of orthogonality between real steering vector and noise subspace. To mitigate the effect of the residual error as much as possible, we may project the steering vector to signal subspace [25]. The projected vector can be formulated as:

$$\hat{\mathbf{p}}_i'(f_d,\tau)=\mathbf{U}_S\left(\mathbf{U}_S^H\mathbf{U}_S\right)^{-1}\mathbf{U}_S^H\mathbf{p}_i\left(f_d,\tau\right)=E_SE_S^H\hat{\mathbf{p}}_i\left(f_d,\tau\right)\quad(24)$$

Since the real steering vectors $\mathbf{p}_i(f_d,\tau)$ $(i=-1,0,1)$ span the same subspace (i.e., signal subspace) as $\mathbf{U}_S=[\beta_s^{(1)},\beta_s^{(2)},\beta_s^{(3)}]$ does and are orthogonal to noise subspace, the operation above can improve the accuracy of steering vector by removing the part of error falling into noise subspace.

According to the description in section A, B, C and D, we summarize the data processing of a multi-channel SAR system as a flow chart shown in Figure 4. In the next section, the experimental results of measured data will be presented.

5. EXPERIMENTAL RESULTS

To confirm the validity of the proposed method, real data collected by a tri-channel SAR system is processed in this section. As mentioned in Section 2, PRF is only one third of Doppler bandwidth in the system.

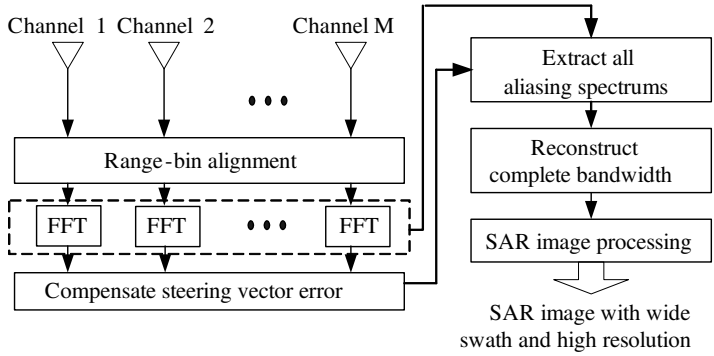

Figure 4. Implementation structure of the proposed method.

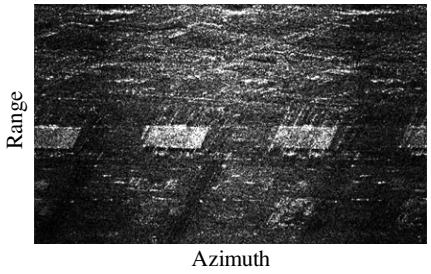

Figure 5. SAR image obtained from the ground echoes acquired by one channel.

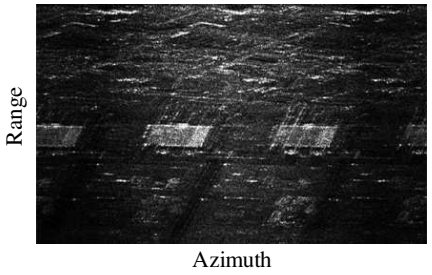

Figure 6. Processing result after STAP-based approach is implemented.

Figure 7. Processing result after error compensation.

Figure 8. Processing result after projection operation.

Figure 5 is the SAR image obtained from the ground echoes acquired by one channel by using conventional SAR imaging operations. Obviously, due to the existence of the Doppler ambiguities there are three profiles for each target in the image. In order to obtain SAR image free of ambiguities, we combine the tri-channel data coherently by using the

STAP-based approach [10]. Figure 6 shows the processing result when the approach above is implemented. During the processing, the impact of any error is not considered. We can see that most of the aliasing components are not suppressed effectively. To improve the quality of SAR image, we estimate and compensate the first kind and the second kind error mentioned in Section 3. Figure 7 is the processing result after step A and step B described in Section 4. As Figure 7 illustrates, the quality of SAR image is improved greatly. Residual steering error, as mentioned above, should be taken into account. Figure 8 is the processing result after step D. Clearly, in comparison with Figure 7, the quality of Figure 8 is further improved.

6. CONCLUSION

Future SAR system will be required to achieve wide area surveillance with high resolution. Multi-channel SAR system is a promising choice. However, there are more deleterious factors in multi-channel SAR system compared to mono-channel SAR system, which may degrade the quality of SAR image greatly. In this paper, all deleterious factors in the system are considered and classified into three kinds according to their impact on Doppler aliasing suppression. And approaches for array error estimation and its compensation are presented, respectively. The validity of the proposed method is demonstrated with real data collected using an experimental tri-channel airborne SAR system.

REFERENCES

1. Moore, R. K. and J. P. Claassen, "Scanning spaceborne synthetic aperture radar with integrated radiometer," *IEEE Trans. Aerospace and Electronic Systems*, Vol. 17, No. 3, 410–421, 1981.
2. Labarre, C, "Wiener filtering applied to magnetic near field scanning," *Progress In Electromagnetics Research*, Vol. 96, 63–82, 2009.
3. Tomiyasu, K., "Image processing of synthetic aperture radar range ambiguous signals," *IEEE Trans. Geoscience and Remote Sensing*, Vol. 35, No. 2, 1114–1117, 1994.
4. Bamler, R. and H. Runge, "PRF ambiguity resolving by wavelength diversity," *IEEE Trans. Geoscience and Remote Sensing*, Vol. 29, No. 6, 997–1003, 1991.
5. Chen, D. and B. Sun, "Multi-wavelength fiber optical parametric oscillator based on a highly nonlinear fiber and a sagnac loop filter," *Progress In Electromagnetics Research*, Vol. 106, 163–176, 2010.

6. Prati, C. and F. Rocca, "Improving slant-range resolution with multiple SAR surveys," *IEEE Trans. Aerospace and Electronic Systems*, Vol. 29, No. 1, 135–143, 1993.
7. Goodman, N. A., S. C. Lin, D. Rajakrishna, et al., "Processing of multiple-receiver spaceborne arrays for wide-area SAR," *IEEE Trans. Geoscience and Remote Sensing*, Vol. 40, No. 4, 841–852, 2002.
8. Krieger, G., N. Gebert, and A. Moreira. "Unambiguous SAR signal reconstruction from nonuniform displaced phase centre sampling," *IEEE Trans. Geoscience and Remote Sensing*, Vol. 1, No. 4, 260–264, 2004.
9. Li, Z., Z. Bao, H. Wang, and G. Liao, "Performance improvement for constellation SAR using signal processing techniques," *IEEE Trans. Aerospace and Electronic Systems*, Vol. 42, No. 2, 436–452, 2006.
10. Li, Z., H. Wang, T. Su, et al., "Generation of wide-swath and high-resolution SAR images from multichannel small spaceborne SAR systems," *IEEE Geoscience and Remote Sensing Letters*, Vol. 2, No. 1, 82–86, 2005.
11. Aguttes, J. P., "The SAR Train concept: Required antenna area distributed over N smaller satellites, increase of performance by N," *Proceedings of IEEE*, Vol. 1, 542–544, 2003.
12. Hong, T., M. Z. Song, and X. Y. Sun, "Design of a sparse antenna array for communication and direction finding applications based on the Chinese remainder theorem," *Progress In Electromagnetics Research*, Vol. 98, 119–136, 2009.
13. Chan, Y. K. and V. C. Koo, "An introduction to synthetic aperture radar (SAR)," *Progress In Electromagnetics Research B*, Vol. 2, 27–60, 2008.
14. Zhao, Y. W., M. Zhang, and H. Chen, "An efficient ocean sar raw signal simulation by employing fast Fourier transform," *Journal of Electromagnetic Waves and Applications*, Vol. 24, No. 16, 2273–2284, 2010.
15. Sekretarov, S. and D. M. Vavriv, "A wideband slotted waveguide antenna array for SAR system," *Progress In Electromagnetics Research M*, Vol. 11, 165–176, 2010.
16. Kim, D. O., N.-I. Jo, H.-A. Jang, and C.-Y. Kim, "Design of the ultrawideband antenna with a quadruple-band rejection characteristics using a combination of the complementary split ring resonators," *Progress In Electromagnetics Research*, Vol. 112, 93–107, 2011.

17. Vazquez Antuna, C., G. Hotopan, S. Ver Hoeye, et al., "Microstrip antenna design based on stacked patches for reconfigurable two dimensional planar array topologies," *Progress In Electromagnetics Research*, Vol. 97, 95–104, 2009.
18. Qu, Y., G. Liao, S.-Q. Zhu, and X.-Y. Liu, "Pattern synthesis of planar antenna array via convex optimization for airborne forward looking radar," *Progress In Electromagnetics Research*, Vol. 84, 1–10, 2008.
19. Li, M, G. Liao, and J. Liu, "Robust elevation prefiltering method for non-side looking airborne radar," *Journal of Electromagnetic Waves and Applications*, Vol. 24, No. 16, 2191–2205, 2010.
20. Choi, G. G., S. H. Park, H. T. Kim, and K. T. Kim, "ISAR imaging of multiple targets based on particle swarm optimization and hough transform," *Journal of Electromagnetic Waves and Applications*, Vol. 23, No. 14–15, 1825–1834, 2009.
21. Yang, P, F. Yang, and Z. P. Nie, "DOA estimation with sub-array divided technique and interporlated esprit algorithm on a cylindrical conformal array antenna," *Progress In Electromagnetics Research*, Vol. 79, 201–216, 2010.
22. Umrani, A. W., "Effect of steering error vector and angular power distributions on beamforming and transmit diversity systems in correlated fading channel," *Progress In Electromagnetics Research*, Vol. 105, 383–402, 2010.
23. Wu, B. I., M. C. Yeung, Y. Hara, and J. A. Kong, "InSAR height inversion by using 3-d phase projection with multiple baselines," *Progress In Electromagnetics Research*, Vol. 91, 173–193, 2009.
24. Errico, M., "Attitude and antenna pointing design of bistatic radar formation," *IEEE Trans. Aerospace and Electronic Systems*, Vol. 39, No. 3, 949–959, 2003.
25. Feldman, D. D. and L. J. Griffiths, "A projection approach for robust adaptive beamforming," *IEEE Trans. Signal Processing*, Vol. 42, No. 4, 867–876, 1994.
26. Ahmed, Y., F. Jawed, S. Zia, and M. S. Aga, "Real-time implementation of adaptive channel equalization algorithms on TMS320C6x DSP processors," *E-Tech 2004*, 101–108, 2004.
27. Kuo, W. C., W. C. Lin, S. C. Lin, and C. M. Lai, "Analog-based detection method in optical low-coherence reflectometer for measurement of retardation and fast-axis angle," *Journal of Electromagnetic Waves and Applications*, Vol. 23, No. 4, 523–533, 2009.